MODEL-BASED MULTI-UAV PATH PLANNING FOR HIGH-QUALITY 3D RECONSTRUCTION OF BUILDINGS

S. Zhang[1]*, W. Zhang[1], C. Liu[2]

[1] School of Geospatial Engineering and Science, Sun-Yatsen University, Zhuhai, China - (zhangsh52,zhangwm25)@mail.sysu.edu.cn
[2] College of Surveying and Geo-informatics, Tongji University, Shanghai, China - liuchun@tongji.edu.cn

KEY WORDS: Multi-UAV, Coarse model, Path planning, 3D reconstruction, Photogrammetric constraints.

ABSTRACT:

Unmanned aerial vehicle (UAV) photogrammetry is widely used for acquiring high-quality 3D models of urban areas. However, the completeness and quality of the reconstructed model can be affected by complex or concave structures when using common flight paths. Furthermore, flight paths with multi-altitude and multi-attitude waypoints can be time-consuming and may not be efficiently implemented by a single drone. To address these challenges, we propose a model-based multi-UAV path planning method for capturing images that enable complete and precise 3D reconstruction of buildings. Our method analyzes the geometry of the input coarse model and plans viewpoints based on the reconstructability related to completeness and precision. By solving a multiple travelling salesmen problem (mTSP), individual flight paths for each UAV are generated. We conducted a real-world experiment comparing the performance and efficiency of the proposed method with two existing solutions. Results the proposed method produces a more complete 3D reconstruction with fewer images compared to the existing methods. It also shows that using two UAVs with the proposed method can significantly reduce the overall time required for 3D reconstruction.

1. INTRODUCTION

Unmanned aerial vehicle (UAV) photogrammetry is a primary method for acquiring high-quality 3D models of urban areas, which serve as spatial references for various urban applications and management tasks, such as construction site monitoring and building information modeling (BIM) (Anwar et al., 2020; Alshawabkeh et al., 2021). Drones equipped with gimbaled cameras offer high maneuverability, enabling them to capture images at close range and from various angles (Nex et al., 2022), resulting in the acquisition of ultra-high resolution 3D models (Cramer et al., 2018). However, when it comes to urban buildings, which often have complex or concave structures, commonly used UAV path planning methods (such as nadir, oblique, or orbit modes) may lead to incomplete or imprecise 3D reconstructions due to self-occlusion (Jiang et al., 2021).

In urban environments, the use of larger or fixed-wing UAVs, which can carry more powerful mapping sensors, is limited due to the complexity of the environment and regulations (Kandeel et al., 2022). On the other hand, small and lightweight drones are more flexible and cost-friendly, making them the preferred choice. However, the limited flying range of small drones restricts their mapping capabilities. Furthermore, these small mapping drones lack smart features such as real-time obstacle avoidance and can only follow pre-planned waypoints. Therefore, allocating the mapping task to multiple UAVs and planning individual waypoints for each UAV is a practical solution to improve the efficiency of data capture for high-quality 3D reconstruction of urban areas (Otto et al., 2018).

Effectively acquiring high-quality 3D models for complex buildings involves two main aspects: fine-grained viewpoint planning and multi-UAV path planning. In terms of viewpoint planning, the challenge of occlusion caused by complex buildings needs to be addressed first (Cabreira et al., 2019). Model-based UAV path planning methods analyze the geometry of the input coarse model (or proxy model), which can be obtained from previous exploration flights (Hepp et al., 2019) or existing models such as satellite reconstructions or BIM (Zhou et al., 2020; Tan et al., 2021). Subsequently, an optimal subset of viewpoints is selected from a candidate set that is uniformly and densely initialized in the navigable space (Roberts et al., 2017). The selection of viewpoints is often guided by a customized *reconstrucability* index, which takes into account factors such as parallax angle, baseline, and ground sampling distance (GSD) in Structure from Motion-Multi-View Stereo (SfM-MVS) theory (Zhang et al., 2020; Peng and Isler, 2019). To address the trade-off between intersection angle and image matching quality, Smith et al. (2019) proposed a parallax weighing function (Wenzel et al., 2013). The problem of viewpoint selection involves non-linear constraints, making it NP-hard, while the objective function is often submodular (Koch et al., 2019). However, the computational complexity can be reduced while maintaining a certain level of global optimality (Krause and Golovin, 2014). Li et al. (2022) formulated a max-min optimization problem to efficiently plan viewpoints in 3D space. Nevertheless, widely used image overlap-based reconstrucability may lead to redundant viewpoint planning and still lacks the guarantee of complete reconstruction. In summary, the reconstrucability index should be carefully designed to balance reconstruction quality and computational cost.

To increase the efficiency of image capture for high-quality 3D reconstruction of buildings, a practical solution is to utilize multi-UAV path planning. In conventional nadir image capture, a boustrophedon coverage flight path is commonly employed. The survey area is divided into sub-regions or sub-strips, with each UAV assigned to cover a specific sub-region (Avellar et al., 2015; Cabreira et al., 2019). However, it is important to note that viewpoints for high-quality 3D reconstruction are irregularly distributed. Therefore, the task allocation of multiple UAVs needs to be carried out at the waypoint

* Corresponding author

level rather than the geometry level. This problem can be formulated as a multiple traveling salesman problem (mTSP) or a vehicle routing problem (VRP). The essence of the problem is that multiple drones start at the same point and need to reach multiple waypoints, with each waypoint being accessed by only one drone. The objective of multi-UAV path planning for high-quality 3D reconstruction is to allocate their paths in order to achieve the lowest total time, shortest total route, or lowest total cost (Coutinho et al., 2018).

For multirotor drones, energy consumption is largely dependent on flight time and has little to do with the attitude of the drone (Liu et al., 2020). Therefore, the main objective of multi-UAV path planning for high-quality 3D reconstruction should be to minimize the total time taken. However, it is important to note that this problem is NP-hard, and commonly used methods such as genetic algorithms and simulated annealing algorithms can only achieve approximate optimization (Aggarwal et al., 2000). Recent advancements in linearization and mixed integer programming have further improved the optimality of the solutions (Staněk et al., 2019). However, for mapping missions, conflicts between UAVs and the buildings should also be considered and resolved.

In this paper, we propose a model-based multi-UAV path planning method for capturing images that enable complete and precise 3D reconstruction. The proposed method analyzes the geometry of the input coarse model and plans viewpoints based on the reconstructability related to completeness and precision. Individual flight paths for each UAV are generated by solving the multiple traveling salesman problem. (Bektas, 2006). The workflow concept is illustrated in Figure 1.

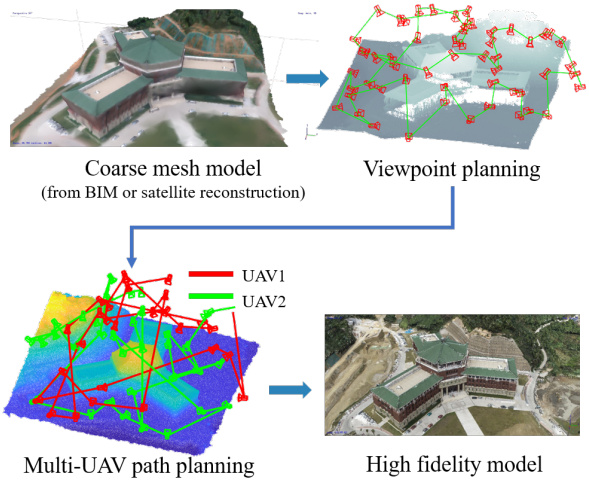

Figure 1. Concept of the proposed method.

2. METHOD

The workflow of the proposed method is illustrated in Figure 2. This method begins by taking a coarse mesh model of the target as input, which can be obtained from BIM (building information modeling) or satellite reconstruction. Candidate viewpoints are then densely initialized in the normal direction of each facet of the target. The distance is calculated using the sensor size, focal length, and the required GSD. Subsequently, the reconstructability of each viewpoint is evaluated by considering factors such as the GSD, baseline, intersection angle, and the estimated error ellipsoid (Zhang et al., 2020). Viewpoints are selected from the candidate viewpoint set to ensure complete coverage of the target, resulting in a *strengthened camera network*. Next, the error ellipsoid of all target points is estimated through photogrammetric forward intersection. Targets with an error ellipsoid larger than the given threshold are identified as low-precision. Additional viewpoints are planned to optimize the viewing geometry of these targets, thereby increasing the reconstruction precision. The viewpoints planned in the previous two steps are combined to form the *optimized camera network*. Finally, the viewpoints are divided and connected to form the flight path for each individual UAV. The details of the workflow are explained as follows.

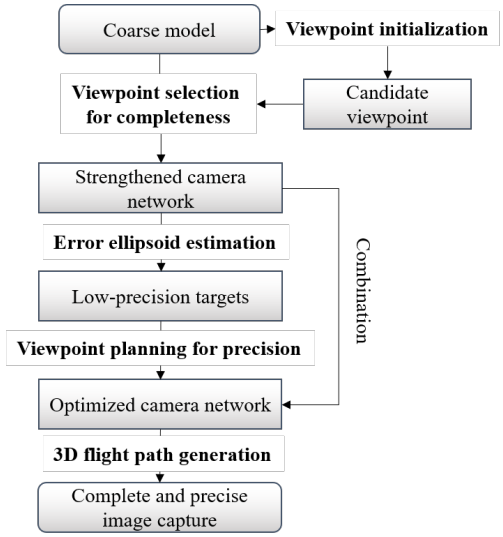

Figure 2. The proposed workflow.

2.1 Viewpoint Selection for Completeness

The viewpoint C in this study has five degrees of freedom, consisting of three degrees of freedom for the position $C^p = \{x, y, z\}$ and two degrees of freedom for the attitude $C^a = \{\phi, \kappa\}$. The roll angle ω of the camera is assumed to be zero due to onboard stabilization. The objective of the viewpoint selection is to choose the minimum number of viewpoints $\mathbf{C_c^*}$ from the candidate set $\mathbf{C_0}$ to fully cover the target surface by planning two viewpoints to observe each sampling point. The viewpoint set $\mathbf{C_c^*}$ should satisfy the objective function and constraints:

$$\begin{aligned} \mathbf{C_c^*} &= \arg\min |\mathbf{C_c}| \\ &\text{s.t. } f(\mathbf{C_c^*}) \geq q \end{aligned} \tag{1}$$

In Equation 1, $|\mathbf{C_c}|$ is the number of viewpoints. $f(\mathbf{C_c^*}) = \sum_{i=1}^{n} R(C_i)$ is the overall reconstructability, and q is the target reconstruction percentage. Considering that there may be highly occluded parts that cannot be observed by the UAV, q can be reduced by a factor of 0.9. $R(C_i)$ is the reconstructability of a viewpoint C_i.

$$R(C_i) = \arg\max \frac{s_o}{s} + \sum_j \sin \psi_j \tag{2}$$

The reconstructability function (Equation 2) considers the ratio of the observed sampling points s_o from viewpoint C to all the points s, and ψ_j is the angle between the light ray direction and the principal direction of the error ellipsoid of point s_j. Other reconstructability factors are transformed into constraints for the optimization problem. The geometry for this viewpoint selection step is shown in Figure 3. The viewpoint candidate (grey) is planned alongside the target point normal n, and its distance to the target d_g depends on the required GSD. m_c is the light ray direction. θ_p is the angle between m_c and n, which is set to 40° according to (Hoppe et al., 2012). N_e is the principal direction of the error ellipsoid, and ψ_i is the angle between m_c and N_e.

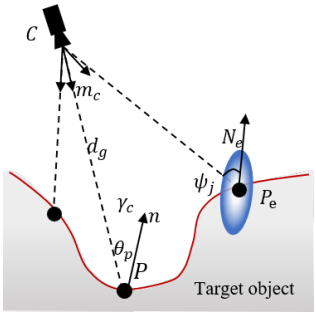

Figure 3. The geometry illustration of viewpoint selection for completeness

2.2 Viewpoint Planning for Precision

This step aims to select additional viewpoints based on the previously strengthened camera network $\mathbf{C_c^*}$ in order to increase precision. The error ellipsoid of each target point s is estimated through multiview intersection. The linearized collinearity equation is given by (Zhang and Hu, 2007):

$$\begin{bmatrix} r_{31}x_{ij}+r_{11}c & r_{32}x_{ij}+r_{12}c & r_{33}x_{ij}+r_{13}c \\ r_{31}y_{ij}+r_{21}c & r_{22}y_{ij}+r_{12}c & r_{33}y_{ij}+r_{23}c \end{bmatrix} \begin{bmatrix} \hat{X}_i - X_{s_j} \\ \hat{Y}_i - Y_{s_j} \\ \hat{Z}_i - Z_{s_j} \end{bmatrix} = 0 \quad (3)$$

Here, $(\hat{X}_i, \hat{Y}_i, \hat{Z}_i)$ are the coordinates of sampling point i, and x_{ij} indicates that sampling point i is observed by viewpoint j. The error ellipsoid can be calculated using the eigenvalues and eigenvectors of the target point (Spruyt, 2015). The size of the semimajor axis m is considered as the theoretical precision of a target point. If m is larger than a threshold, for example $3 \times GSD$, the target point is considered to have low precision. For each selected target point, a new viewpoint C_p is planned to increase precision. The position and attitude of the initialized viewpoint are optimized using the objective function:

$$C_p^* = \arg\max f_p(C,s) + \Psi'(C) \quad (4)$$
$$\text{where } f_p(C,s) = \frac{s_o}{s},\ \Psi'(C) = \sin\psi_i$$

In Equation 4, $\Psi'(C)$ represents the angle between the semimajor axis of the error ellipsoid and the direction of the light ray. Therefore, $f_p(C,s)$ promotes the observation of the viewpoint from more sampling points and increases the precision of the target point simultaneously. It plans the viewpoint with a large intersection angle to increase precision. Figure 4 demonstrates the geometry, illustrating the optimization of precision. The planned viewpoint C_p is also constrained by the distance d_g and intersection angle θ_p.

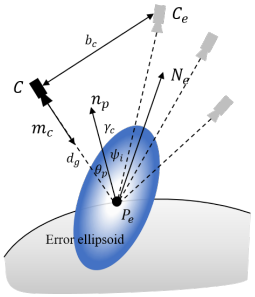

Figure 4. The geometry illustration of viewpoint planning for precision.

The new viewpoints planned in this step, $\mathbf{C_p}$, are finally combined with the viewpoints for completeness, $\mathbf{C_c}$, to form the final *optimized camera network* for UAV path generation $\mathbf{C_r} = \mathbf{C_c} \bigcup \mathbf{C_p}$.

2.3 Path Generation for Multiple UAVs

This step involves planning flight paths for n_d UAVs using the camera network $\mathbf{C_r}$ obtained from the previous steps. We assume that the UAVs are multirotor drones equipped with gimbal cameras, allowing them to fly in 3D space and capture images from various attitudes by yawing and rotating the gimbal.

To begin, we construct a graph $G(V,E)$ where each viewpoint C_r in the set $\mathbf{C_r}$ corresponds to a vertex V. The edges E represent the cost between vertices. Assuming there are n UAVs required to traverse all viewpoints in $\mathbf{C_r}$, the takeoff positions for each UAV are denoted as $\mathbf{S} = \{S_1, S_2, ..., S_n\}$, where $\forall S_i \notin \mathbf{C_r}$. The path for the ith UAV is denoted as $\mathbf{P_i} = \{S_1, E_1, ..., E_k \in \mathbf{E}, S_1\}$, indicating that the UAV takes off from S_i, follows the edges E_k, and returns to the takeoff position. We define the set of break-points $\mathbf{B} = [B_1, B_2, ...B_{n-1}]$ to divide the path $\mathbf{P}$ into $\mathbf{P_i}$ segments.

The objective of using multiple UAVs for the flight path is to save time. For multirotor UAVs, the flight time is primarily determined by the length of the path (Liu et al., 2020). Therefore, we set the cost E as the Euclidean distance between vertices, and the objective function is to minimize the overall length:

$$\min \sum_{i=1}^{n} L(P_i) \quad (5)$$

where $L(P_i)$ represents the length of the ith path. Assuming that the maximum flying range of each drone is d_m, we introduce a penalty coefficient k_d to adjust the distance correlation function beyond the range path. This adjustment effectively modifies the value of the objective function to increase the constraint:

$$L(P_i) = \begin{cases} L(P_i) & L(P_i) \le d_m \\ k_d(L(P_i) - d_m) + d_m & L(P_i) > d_m \end{cases} \quad (6)$$

In Equation 6, if the path for a certain UAV exceeds the range, the cost of its excess part increases by a factor of k_d. If an

obstacle is present between two vertices, the distance is adjusted using an obstacle-avoidance trajectory, which can be planned using an algorithm such as A*. Finally, a multiple traveling salesmen problem is formulated and solved on the graph G to obtain the flight path for each UAV.

3. EXPERIMENT AND RESULTS

A real-world experiment was conducted to evaluate the performance and efficiency of the proposed method. The experiment compared the proposed method with the Nap-of-the-object photogrammetry planning (NFP) method (Wang et al., 2022) and Agisoft Metashape's method (MS) (Agisoft LLC, 2022). The target building was a multipart Chinese-style building with dimensions of approximately 155×155 m. A lower-resolution model reconstructed from nadir UAV images was used to simulate the input satellite model. Two DJI Phantom 4 RTK drones were used for image capture, with an average capture distance of 30 m and a GSD of approximately 1.5 cm. The overlap settings for NFP and Metashape were set to 65%. The sidelap for NFP was set to 50%, while Metashape does not provide such a setting. Figure 5 shows the viewpoints planned by each comparing method. Agisoft Metashape was used for model reconstruction.

To evaluate the absolute accuracy, 20 reference points were signalized with the real-time kinematic (RTK) system, and 5 of them were ground control points (GCPs) (Figure 6). The ground truth model was reconstructed from oblique imaging and georeferenced with all reference points, ensuring high completeness and accuracy.

Table 1 presents the properties of the flight paths. The proposed method planned only 62 images, while NFP planned 169 images and MS had 192 images, resulting in the longest flight path. The flight time was significantly lower for the proposed method due to the fewer viewpoints. The "Proposed-DUAL" paths were implemented by individual drones (No. 1 and 2), which saved approximately 160 seconds compared to a single drone.

Table 1. Flight path comparison.

Name	# of images	Length(m)	Flight time (s)
NFP	169	2300	1667
MS	192	2814	1874
Proposed	62	1746	549
Proposed-DUAL-1	28	1674	354
Proposed-DUAL-2	34	1575	384

The visual comparison of the dense image matching (DIM) point cloud is shown in Figure 7. The reconstruction from NFP's method has many defects on the green roof and red façade, while the proposed method produces a more complete result with only some defects on the roof. The MS path with 192 images appears to be the most complete one. The strip-like viewpoint distribution of NFP's method may not be as good as the even distribution achieved by Metashape's method. The Proposed-DUAL method had exactly the same viewpoints as the Proposed method, but it was implemented with two drones working collaboratively. There was one more set of interiors to solve, and the reconstruction looks similar to that from a single drone.

The DIM point cloud from each flight path was compared with the reference model, and the quantitative results are demonstrated using three indicators: precision, recall, and F1-score. Precision P quantifies the number of reconstructed points that are close to the ground truth points, while recall R quantifies the number of ground truth points that are close to a reconstructed point, which can also be interpreted as the completeness and an indicator of the overall absolute accuracy. The F1-score, $F = \frac{2PR}{P+R}$, can be used as a performance measure for 3D reconstruction (Hepp et al., 2019). Table 2 presents the results. The quantitative results align with the visual comparison. Among all three flight paths, the proposed method achieves the best results for all three indicators. The NFP method has a higher precision but lower recall compared to the MS method, despite using fewer images. The strip-like viewpoints of the NFP method may assist in accurate image matching and exterior estimation, resulting in better precision. Compared to the single drone method, the results from the two drones method (Proposed-DUAL) are slightly lower, possibly due to the introduction of another set of camera interior.

Table 2. Quantitative comparison of DIM point cloud.

Name	Precision (%)	Recall (%)	F1-score
NFP	36.26	26.91	0.309
MS	34.94	28.42	0.313
Proposed	**41.32**	**30.30**	**0.350**
Proposed-DUAL	40.98	29.90	0.346

Regarding the absolute accuracy, we compared the errors in the XY, Z, and total dimensions for the checkpoints. The results are presented in Table 3. It is worth noting that the XY errors obtained from all flight paths are relatively large, considering the centimeter-level GSD. This might be attributed to systematic errors between the reference points and the initial exteriors obtained from the drone. All the compared methods yielded similar results, with only a few centimeters of difference. However, the proposed flight path implemented with two drones exhibited slightly better performance in terms of XY and total error.

Table 3. Absolute error comparison via checkpoints (cm)

Name	XY error	Z error	Total
NFP	48.35	8.98	49.18
MS	40.95	**5.40**	41.30
3D	42.99	6.23	43.44
3D-DUAL	**40.38**	5.69	**40.78**

4. CONCLUSIONS

In this paper, we proposed a model-based multi-UAV path planning method for capturing high-quality 3D reconstructions of buildings. The proposed method utilizes a coarse model as input and incorporates photogrammetric constraints and error ellipsoids to guide viewpoint selection. The flight paths for multiple UAVs are then planned by solving a multiple traveling salesman problem. The results demonstrate that the proposed method achieves a more comprehensive 3D reconstruction using fewer images compared to existing methods such as NFP and Metashape. Additionally, the efficiency of image capture is increased through the planning of paths for multiple UAVs.

However, there are still some limitations that need to be addressed. Firstly, the proposed method assumes that the input coarse model is error-free. In practice, the coarse model may contain errors up to several meters, which can impact the quality and safety of the reconstruction. Therefore, future work will consider the uncertainty associated with the input model.

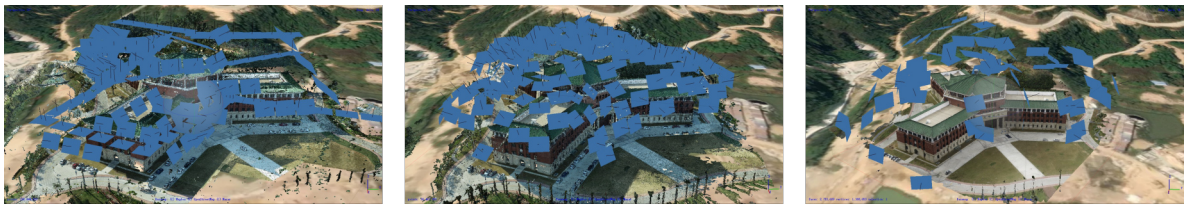

NFP MS Proposed

Figure 5. Planned viewpoints of the experiment.

Figure 6. The target building and reference points of the experiment. Red points indicate GCPs.

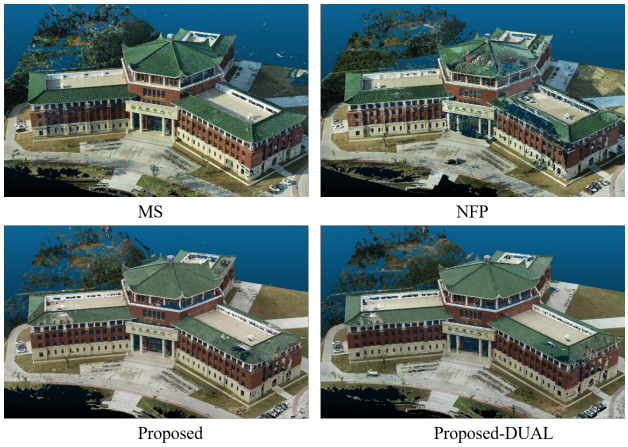

MS NFP

Proposed Proposed-DUAL

Figure 7. Comparison of DIM point clouds.

Secondly, the current multi-UAV path generation method only considers obstacle avoidance. However, there may be potential conflicts between UAVs during operation, necessitating mission planning that avoids collisions between UAVs. To address this, future work will introduce additional dynamic constraints to ensure safety.

5. ACKNOWLEDGEMENTS

The research in this paper was supported by the Fundamental Research Funds for the Central Universities, Sun Yat-sen University (Grant No. 23ptpy98).

References

Aggarwal, A., Coppersmith, D., Khanna, S., Motwani, R., Schieber, B., 2000. The angular-metric traveling salesman problem. *SIAM Journal on Computing*, 29(3), 697–711.

Agisoft LLC, 2022. Mission planning for complex structures.

Alshawabkeh, Y., Baik, A., Miky, Y., 2021. Integration of Laser Scanner and Photogrammetry for Heritage BIM Enhancement. *ISPRS International Journal of Geo-Information*, 10(5), 316.

Anwar, N., Izhar, M. A., Najam, F. A., 2020. Construction Monitoring and Reporting using Drones and Unmanned Aerial Vehicles (UAVs). *The Tenth International Conference on Construction in the 21st C*, 9.

Avellar, G. S. C., Pereira, G. A. S., Pimenta, L. C. A., Iscold, P., 2015. Multi-UAV Routing for Area Coverage and Remote Sensing with Minimum Time. *Sensors*, 15(1111), 27783–27803.

Bektas, T., 2006. The Multiple Traveling Salesman Problem: An Overview of Formulations and Solution Procedures. *Omega*, 34(3), 209–219.

Cabreira, T. M., Brisolara, L. B., Ferreira Jr., P. R., 2019. Survey on Coverage Path Planning with Unmanned Aerial Vehicles. *Drones*, 3(1), 4.

Coutinho, W. P., Battarra, M., Fliege, J., 2018. The unmanned aerial vehicle routing and trajectory optimisation problem, a taxonomic review. *Computers & Industrial Engineering*, 120, 116–128.

Cramer, M., Haala, N., Laupheimer, D., Mandlburger, G., Havel, P., 2018. Ultra-High Precision UAV-based LiDAR and Dense Image Matching. *ISPRS - International Archives of the Photogrammetry, Remote Sensing and Spatial Information Sciences*, XLII-1, 115–120.

Hepp, B., Nießner, M., Hilliges, O., 2019. Plan3D: Viewpoint and Trajectory Optimization for Aerial Multi-View Stereo Reconstruction. *ACM Transactions on Graphics*, 38(1), 1–17.

Hoppe, C., Wendel, A., Zollmann, S., Pirker, K., Irschara, A., Bischof, H., Kluckner, S., 2012. Photogrammetric Camera Network Design for Micro Aerial Vehicles. *Computer Vision Winter Workshop: CVWW 2012*, Mala Nedelja, Slovenia, 9.

Jiang, S., Jiang, W., Wang, L., 2021. Unmanned Aerial Vehicle-Based Photogrammetric 3D Mapping: A Survey of Techniques, Applications, and Challenges. *IEEE Geoscience and Remote Sensing Magazine*, 2–38.

Kandeel, M. E., Salameh, H. A. B., Elrefae, G. A., Qasim, A., 2022. Regulations for UAV Operation in Social Applications and Services: A General Perspective. *2022 Ninth International Conference on Social Networks Analysis, Management and Security (SNAMS)*, 1-6.

Koch, T., Körner, M., Fraundorfer, F., 2019. Automatic and Semantically-Aware 3D UAV Flight Planning for Image-Based 3D Reconstruction. *Remote Sensing*, 11(13), 1550.

Krause, A., Golovin, D., 2014. Submodular Function Maximization. *Tractability: Practical Approaches to Hard Problems*, Cambridge University Press, Cambridge, 71–104.

Li, Q., Huang, H., Yu, W., Jiang, S., 2022. Optimized Views Photogrammetry: Precision Analysis and a Large-Scale Case Study in Qingdao. *IEEE Journal of Selected Topics in Applied Earth Observations and Remote Sensing*, 1–17.

Liu, C., Akbar, A., Wu, H., Zhou, Y., Zhang, S., 2020. Mission Capability Estimation of Multicopter UAV for Low-Altitude Remote Sensing. *Journal of Intelligent & Robotic Systems*, 100(2), 667–688.

Nex, F., Armenakis, C., Cramer, M., Cucci, D., Gerke, M., Honkavaara, E., Kukko, A., Persello, C., Skaloud, J., 2022. UAV in the Advent of the Twenties: Where We Stand and What Is Next. *ISPRS Journal of Photogrammetry and Remote Sensing*, 184, 215–242.

Otto, A., Agatz, N., Campbell, J., Golden, B., Pesch, E., 2018. Optimization approaches for civil applications of unmanned aerial vehicles (UAVs) or aerial drones: A survey. *Networks*, 72(4), 411–458.

Peng, C., Isler, V., 2019. Adaptive View Planning for Aerial 3D Reconstruction. *2019 International Conference on Robotics and Automation (ICRA)*, 2981–2987.

Roberts, M., Dey, D., Truong, A., Sinha, S., Shah, S., Kapoor, A., Hanrahan, P., Joshi, N., 2017. Submodular trajectory optimization for aerial 3D scanning. *Proceedings of the IEEE International Conference on Computer Vision (ICCV)*, Venice, Italy, 5324–5333.

Smith, N., Moehrle, N., Goesele, M., Heidrich, W., 2019. Aerial Path Planning for Urban Scene Reconstruction: A Continuous Optimization Method and Benchmark. *ACM Transactions on Graphics*, 37(6), 1–15.

Spruyt, V., 2015. How to draw an error ellipse representing the covariance matrix.

Staněk, R., Greistorfer, P., Ladner, K., Pferschy, U., 2019. Geometric and LP-based heuristics for angular travelling salesman problems in the plane. *Computers & Operations Research*, 108, 97–111.

Tan, Y., Li, S., Liu, H., Chen, P., Zhou, Z., 2021. Automatic Inspection Data Collection of Building Surface Based on BIM and UAV. *Automation in Construction*, 131, 103881.

Wang, W., Zhao, W., Chai, B., Du, J., Tang, L., Yi, X., 2022. Discontinuity Interpretation and Identification of Potential Rockfalls for High-Steep Slopes Based on UAV Nap-of-the-Object Photogrammetry. *Computers & Geosciences*, 166, 105191.

Wenzel, K., Rothermel, M., Fritsch, D., Haala, N., 2013. IMAGE ACQUISITION AND MODEL SELECTION FOR MULTI-VIEW STEREO. *ISPRS - International Archives of the Photogrammetry, Remote Sensing and Spatial Information Sciences*, XL-5/W1, 251–258.

Zhang, J., Hu, A., 2007. Method and Precision Analysis of Multi-Baseline Photogrammetry. *Geomatics and Information Science of Wuhan University*, 32(10), 847–851.

Zhang, S., Liu, C., Haala, N., 2020. Three-Dimensional Path Planning of UAVs Imaging for Complete Photogrammetric Reconstruction. *ISPRS Annals of the Photogrammetry, Remote Sensing and Spatial Information Sciences*, V-1-2020, 325–331.

Zhou, X., Xie, K., Huang, K., Liu, Y., Zhou, Y., Gong, M., Huang, H., 2020. Offsite Aerial Path Planning for Efficient Urban Scene Reconstruction. *ACM Transactions on Graphics*, 39(6), 1–16. https://doi.org/10.1145/3414685.3417791.